

First results from plasma edge biasing on SPECTOR

Carl Dunlea^{1*}, General Fusion Team²,
Chijin Xiao¹, and Akira Hirose¹

¹University of Saskatchewan, Saskatoon, Canada

²General Fusion, Vancouver, Canada

*e-mail: cpd716@mail.usask.ca

Abstract

A description of an edge-biasing experiment conducted on the SPECTOR (Spherical Compact Toroid) plasma injector is presented, along with initial results. The insertion of a disc-shaped molybdenum electrode (probe), biased at up to +100V, into the edge of the CT (Compact Torus), resulted in up to 1kA radial current being drawn. Core electron temperature, as measured with a Thomson-scattering diagnostic, was found to increase by a factor of up to 2.4 in the optimal configuration tested. H_α intensity was observed to decrease, and CT lifetimes increased by a factor of up to 2.3. A significant reduction in electron density was observed; this is thought to be due to the effect of a transport barrier impeding CT fueling, where, as verified by MHD simulation, the fueling source is neutral gas that remains concentrated around the gas valves after CT formation.

1 Introduction

High confinement mode (H-mode) has been implemented by various means (*e.g.*, edge biasing, neutral beams, ion or electron cyclotron heating, lower hybrid heating, and ohmic heating) on a range of magnetic confinement configurations including tokamaks, reversed field pinches, stellarators, and mirror machines. The first H-mode was produced in the ASDEX tokamak by neutral beam injection in 1982 [1]. In 1989, H-mode was first produced by electrode edge biasing on the CCT tokamak [2, 3]. In 1990, it was observed that edge impurity ion poloidal speed is modified abruptly during transitions from low to high confinement modes on the DIII-D tokamak [4]. H-mode has been produced routinely on many magnetic-fusion experiments, including practically all the large tokamaks, for example JET, TFTR, and JT-60. Since the initial electrode-biasing experiments on CCT, H-mode has been produced by edge biasing on many tokamaks, for example CASTOR [5, 6], T-10 [6, 7], STOR-M [8], ISTTOK [9], TEXTOR [6, 10], J-TEXT [11], and TCABR [12].

Electrode biasing involves the insertion of an electrode, that is biased relative to the vessel wall near the point of insertion, into the edge of a magnetized plasma. This leads to a radially directed electric field between the probe and the wall. A commonly held interpretation of the mechanism behind the improved confinement observed on edge biasing experiments is that the resultant $\mathbf{J}_r \times \mathbf{B}$ force imposed on the plasma at the edge of the plasma confinement region varies with distance between the probe and the wall, because E_r , as well as the magnetic field, vary in that region. The associated torque

overcomes viscous forces, spinning up the edge plasma, and results in shearing of the particle velocities between the probe and the wall. The sheared velocity profile is thought to suppress the growth of turbulent eddies that advect hot plasma particles to the wall, thereby reducing this plasma cooling mechanism. In general, H-modes induced by probe biasing share features of those initiated by various methods of heating, including a density pedestal near the wall (near the probe radius for probe biasing), diminished levels of recycling as evidenced by reduced H_α emission intensity, and increased particle and energy confinement times. For example, increases in energy confinement times by factors of 1.5, 1.5, 1.2, 1.8 and 2 were reported for CCT, STOR-M, TEXTOR, T-10 and TCABR respectively. Core electron density increased by a factor of four on CCT, while line-averaged electron density increased by factors of 2, 2, 1.5, 1.8 and 2.6 on STOR-M, TEXTOR, T-10, CASTOR and TCABR respectively. Of these six examples, a biasing-induced temperature increase was noted only for the T-10 experiment, with an increase in core ion temperature by a factor of 1.4 reported, while reduced H_α emission intensity was recorded in each case. Many of these biasing experiments [2, 3, 8, 10, 12] have probed the plasma edge region, obtaining profiles of, for example, electric field, density, temperature and/or velocity profiles, leading to clarifications of the mechanisms involved in the transition to H-mode.

Positive as well as negative electrode biasing works well on some machines; in other instances only one biasing polarity has the desired effect. Most biasing experiments have used passive electrodes, while some have implemented electron-emitting electrodes. Emissive electrodes have, in addition to a circuit to bias the electrode relative to the vacuum vessel, a separate heating circuit, and are heated until they emit electrons. Materials traditionally used for emissive electrodes include lanthanum hexaboride (LaB6) and tungsten (W). Generally speaking, emissive electrodes add complexity to an experiment, but may be beneficial when the edge plasma electron density is so low that dangerously high voltages (which could initiate a current arc that could damage the electrode and vessel) would be required in order to draw an edge current sufficiently high enough for the $\mathbf{J}_r \times \mathbf{B}$ force to overcome inertial effects (viscosity, friction) and drive edge rotation. In the CCT tokamak [2], LaB6 cathodes heated by carbon rods drew edge current up to 40A when the voltage measured between the electrode (probe) and vessel wall was $V_{probe} \sim -250\text{V}$. On CCT, for negative bias, it was found that both electron-emissive electrodes and passive graphite electrodes produced similar results, as long as the electrode was large enough to draw sufficient current ($\sim 20\text{A}$), and small enough not to form a limiter [2]. For negative biasing on ISTTOK, it was not possible to draw more than 2 to 3A with a passive electrode, compared with $\sim 20\text{A}$ with an emissive electrode, while the current drawn with positive biasing was the same for emissive and non-emissive electrode ($I_{probe} \sim 28\text{A}$ at $V_{probe} \sim +130\text{V}$).

It is widely accepted that radial electric fields at the edge plasma, and mitigation of turbulent transport, are involved in the transition between L and H modes in tokamaks. However, an issue that has been widely considered is whether it is the direct stabilization of a turbulence-inducing plasma instability, by enhanced velocity shear in the transport barrier, or actual eddy decorrelation and direct energy transport reduction at the barrier, that causes the confinement improvements that are routinely observed in H-modes. H-modes produced by electrode biasing support the theory that it is actual eddy decorrelation that leads to the radial transport reduction. In these cases, the experimenter controls E_r , the radial component of the electric field, and velocity shear directly. However, in a magnetized plasma, stabilization of a range of modes can occur if $\omega_{E \times B}$, the $E \times B$ shearing rate, is greater than ω_{max} , the maximum linear growth rate of the mode [13, 14]. Interaction between the unstable mode with a nearby stable mode can lead to enhanced Landau damping of the unstable mode [13]. Nonlinear gyro-Landau fluid simulations indicate turbulence stabilization in cases where $\omega_{E \times B}$ is comparable to ω_{max} , the maximum linear growth rate of all the unstable modes in the plasma [15]. According to [13], for a significant reduction of turbulence, it is not a strict requirement that $\omega_{E \times B} > \omega_{max}$ for all unstable modes in the plasma, just that $\omega_{E \times B}$ must be at least of the order of the nonlinear saturation of the turbulence level due to all modes. Note that $\omega_{E \times B}$ enters into the various theories quadratically [14], so that its sign is irrelevant. H-mode has been observed experimentally with both signs of E_r and $\omega_{E \times B}$. The

Ion Temperature Gradient (ITG) mode is thought to contribute to turbulence initiation and thermal transport in magnetically confined plasmas, in particular in plasmas with high ion temperatures and sufficiently weak density profiles [16]. Nonlinear numerical analysis has shown that the ITG mode is completely suppressed when $\omega_{E \times B} \sim \omega_{max}$ [13].

For decorrelation of turbulence due to $E \times B$ shear, $\omega_{E \times B}$ must be of the order of $\Delta\omega_T$, the turbulence decorrelation rate associated with turbulent radial diffusion of fluctuations by the ambient turbulence [13, 14]. $\Delta\omega_T$ can be calculated in some cases but it is not generally available for comparison with experiment. It has been shown by theoretical analysis that, contrary to expectation, a radial electric field without dependence on the radial coordinate, can actually result in a differential rotation (*i.e.*, sheared $E \times B$ velocity) as a result of geometric effects [17]. In that work, by studying the development and saturation of resistivity-gradient-driven turbulence in the presence of a radial electric field in cylindrical geometry, the authors concluded that the turbulence decorrelation rate was not modified when $\omega_{E \times B} \lesssim \Delta\omega_T$. In a consequent publication by a different group [18], it was shown analytically that coupling between poloidal shearing and turbulent radial scattering can account for turbulence quenching without invoking model-dependent, symmetry breaking effects such as diamagnetic rotation. The researchers showed that if an E_r (of either sign) with sufficient radial shear (in either direction), can be established one way or another, that this would lead to turbulence suppression. They emphasized that it is a combination of radial scattering and poloidal shearing, with a weighting on poloidal shearing, that determines the turbulence decorrelation process. They suggest that, since the radial decorrelation length for several turbulence models scales inversely with magnetic field, that it is more difficult to suppress turbulence when the magnetic field is high. Theory predicts that an adequate $E \times B$ shearing rate results in reduction of radial, fluctuation-driven transport. Supporting this, plasma edge Langmuir probe measurements, for electrode biasing-induced H-modes as well as for spontaneous H-modes in tokamaks and in the Wendelstein 7-AS stellarator, show large reductions in fluctuation-driven particle flux [19].

Pre-biasing conditions of radial electric field and an extensive range of plasma parameters play roles in determining the beneficial polarity and the level of bias-induced plasma confinement improvement [13]. A reduction of radial transport at the edge would be beneficial for confinement not only because of reduced outward thermal transport, but also due to reduced inward transport of cold wall-recycled particles to the core. This latter effect is especially relevant on small machines (such as SPECTOR, major radius $R \sim 19\text{cm}$, minor radius $a \sim 8\text{cm}$, no limiter or divertor) for which the surface area to volume ratio of the magnetically confined plasma is large, particularly in configurations without a limiter or divertor, where the recycling process is more important.

An overview of the experiment setup with a description of the biasing electrode assembly is presented in section 2. Circuit analysis, leading to an estimate for the resistance of the plasma between the electrode and flux conserver, which was useful for optimising the circuit, is the focus of section 3. Main results are presented in section 4. A discussion of principal findings, conclusions and possible further improvements to the experiment is presented in section 5. Results from simulations of neutral and plasma fluid interaction during CT formation in SPECTOR geometry is presented in appendix A. The simulations indicate that neutral gas, which remains concentrated around the locations of the machine gas valves after CT formation, can diffuse up the gun as a source of CT fueling. It may be partly due to the effect of a transport barrier impeding the CT fueling process that the improvements in confinement times and electron temperatures observed with the initial edge biasing tests on SPECTOR appear especially significant.

2 Experiment setup

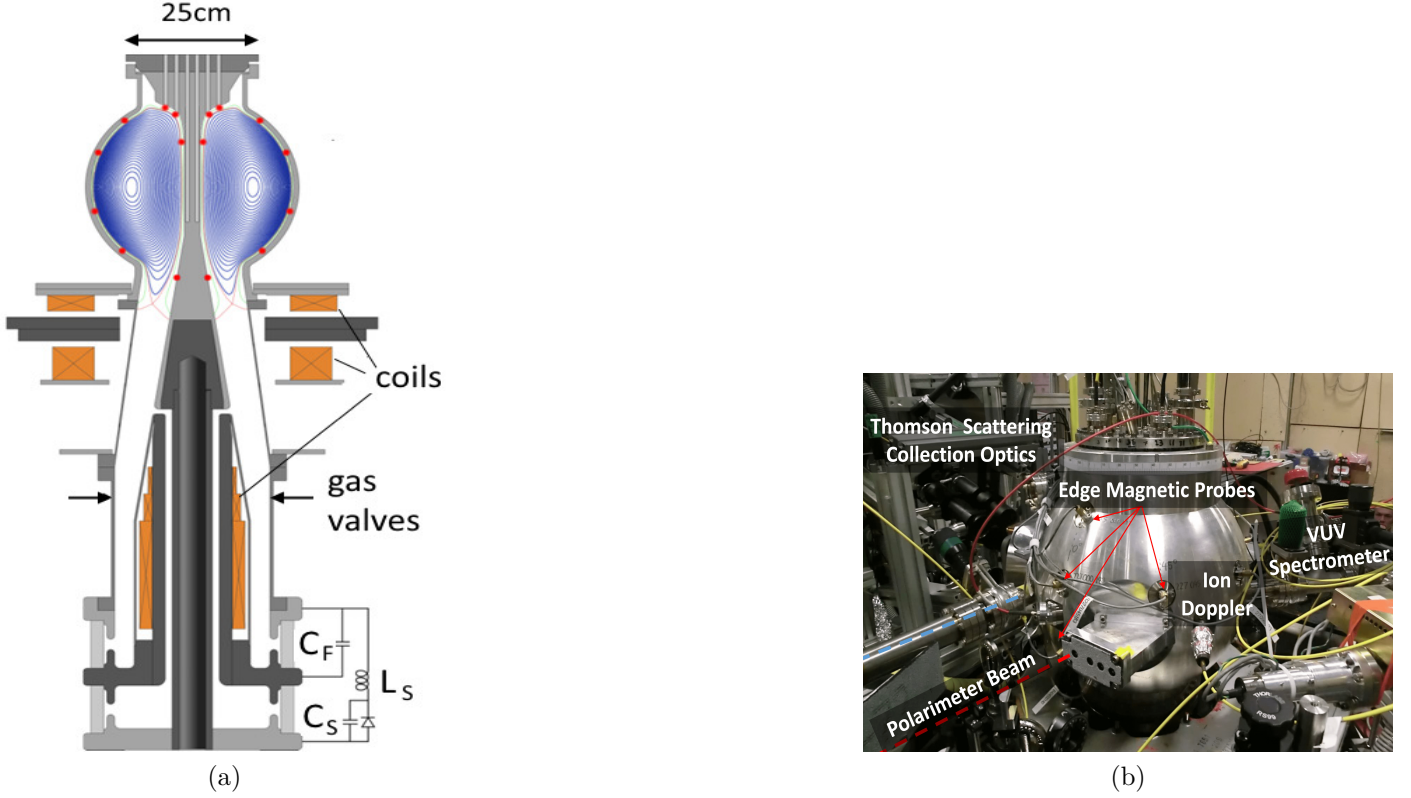


Figure 1: Schematics of SPECTOR plasma injector and diagnostics

A schematic of the SPECTOR [20] plasma injector is depicted in figure 1(a), where the red dots along the flux conserving wall of the CT containment region represent the locations of magnetic probes. SPECTOR is a magnetized Marshall gun that produces compact tori (CTs). It has, in addition to the formation circuit that drives up to 0.8MA formation current over around 80 μ s, a separate circuit to produce an approximately constant shaft current of up to 0.5MA, which flows up the outer walls of the machine and down the central shaft, increasing CT toroidal field and making the CT more robust against MHD instability. Shaft current duration is extended to around 3ms with a crowbar inductor/diode circuit, which is indicated schematically in figure 1(a). Toroidal field at the CT core is typically around 0.5T. The low CT aspect ratio, and the q profile, define the CTs as spherical tokamaks. Initial poloidal flux on the SPECTOR injector is up to 30 mWb. Coaxial helicity injection produces plasma currents in the range 0.3 – 0.8MA. SPECTOR has a range of plasma diagnostics including magnetic probes, visible and VUV spectroscopy, three interferometer chords, multi-point Thomson scattering (TS), and a four chord FIR polarimeter system. The plasma facing components are mostly plasma-sprayed tungsten and bare aluminum, and can be coated with lithium as a gettering agent. Experimental investigations of formation dynamics, MHD mode activity, evolution of plasma profiles, and machine operation setting optimisation have been made. Safety factor profiles can be controlled by varying shaft current and the axial distribution of poloidal gun flux. Thomson-scattering (TS) measurements have indicated CT electron temperatures in excess of 400eV and densities of the order 10^{20} m^{-3} . Energy confinement times of the order of 100 ms have been estimated [20]. A selection of TS system-produced electron temperature and electron density measurements [21] (both taken at 300 μ s after CT formation), electron density measurements obtained with a far-infrared (FIR) interferometer [22], spectral data, and magnetic

probe data, will be presented in this paper. The principal diagnostics are indicated in figure 1(b).

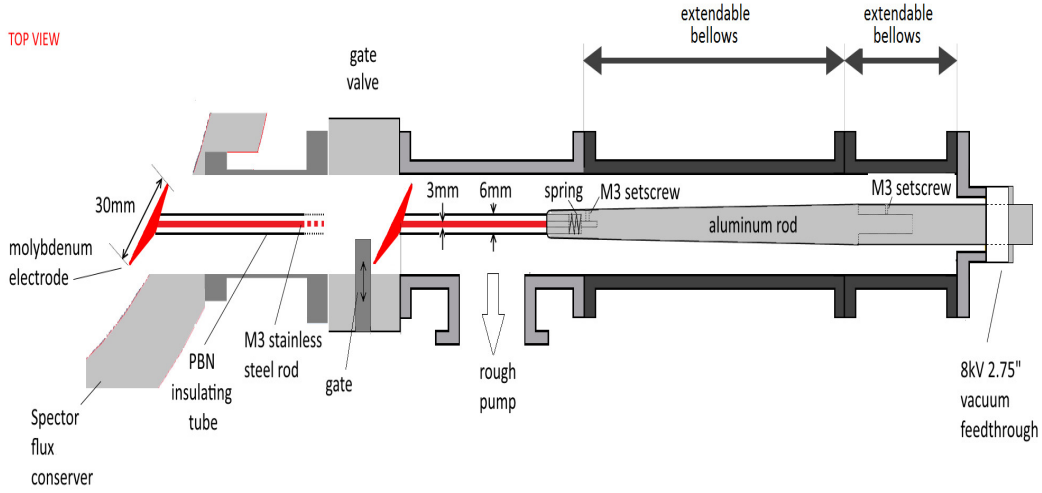


Figure 2: Biasing probe assembly

Figure 2 indicates a top-view of the electrode (probe) assembly with extendable vacuum bellows. The biasing electrode can be retracted behind the gate valve and isolated from the machine vacuum. The approximately disc-shaped electrode (tapered towards the flux-conserver facing side to enable attachment to the steel rod, as indicated in figure 2) is machined from molybdenum bar. It has a 30mm diameter and has an average thickness of approximately 3mm. Molybdenum was chosen for its high work function against sputtering, high melting point, and its resilience against the corrosive action of lithium, which is used as a gettering agent on SPECTOR. A pyrolytic boron nitride (PBN) tube is used as a plasma-compatible insulator around the M3 stainless steel rod that connects the electrode to a tapered aluminum rod, which is in turn connected to the 0.5 inch diameter copper rod that forms part of the 8kV 2.75 inch CF (ConFlat) vacuum feedthrough. The electrode can be inserted up to 45mm into the vacuum vessel; insertion depth was 11mm for the results presented here. Note that the probe can be used as a limiter by connecting the vacuum feedthrough indicated in figure 2 directly to the vacuum vessel. This configuration was not tested because tests using a molybdenum limiter on other GF injectors resulted in evidence of localised limiter melting.

3 Circuit analysis

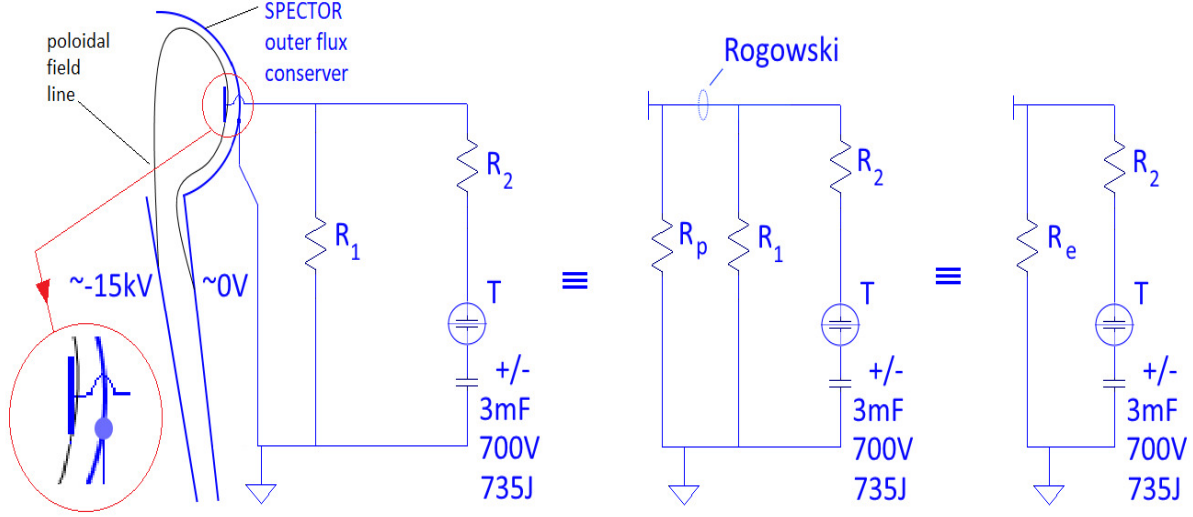


Figure 3: Biasing probe circuit schematic. Note the inset on the lower left of the figure depicts the connection of the circuit to the flux conserver and probe.

Figure 3 indicates the most optimal of the biasing probe circuit configurations tested. The biasing circuit was kept open-circuited until well after CT formation, in order to protect biasing circuit components. A thyatron switch (indicated in the figure) is robust against large amplitude negative voltage spikes that can appear on the probe during CT formation when initially open stuffing-field lines, that are resistively pinned to the injector inner and outer electrodes, intersect the probe (see left subfigure). These thyatron switches are designed to operate at several kilovolts, and usually require several kiloamps of current to remain closed, but careful setting of switch temperature enabled operation at moderate voltages and currents. The biasing capacitor voltage setting V_{bc0} , parallel and series resistors R_1 and R_2 , and R_p , the plasma resistance between the electrode (*i.e.*, probe) and flux conserver, determine V_{probe} , the voltage measured between the probe and flux conserver, and I_{probe} , the current drawn through the plasma edge. The current drawn has a radial component, which leads, in the classical edge biasing scenario, to $\mathbf{J}_r \times \mathbf{B}$ driven edge velocity shearing and consequential decorrelation of turbulence cells and confinement improvement. For the circuit with the 3mF capacitor depicted in figure 3, optimal circuit resistances were found to be $R_1 \sim 0.2\Omega$, and $R_2 \sim 0.5\Omega$. Negative electrode biasing was briefly tested; the results presented in this paper were obtained with positive biasing. The effective resistance R_e , comprised of R_p and R_1 in parallel (see figure 3, right subfigure), is given by

$$R_e(t) = \frac{R_p(t) R_1}{R_p(t) + R_1} \quad (1)$$

The voltage applied by the capacitor on the probe is

$$V_{applied}(t) = V_{bc}(t) \left(\frac{R_e(t)}{R_e(t) + R_2} \right) \quad (2)$$

where $V_{bc}(t)$ is the voltage across the biasing capacitor. Equations 1 and 2 can be combined to provide an expression for R_p :

$$R_p(t) = \frac{R_1 R_2 V_{applied}(t)}{R_1 (V_{bc}(t) - V_{applied}(t)) - V_{applied}(t) R_2} \quad (3)$$

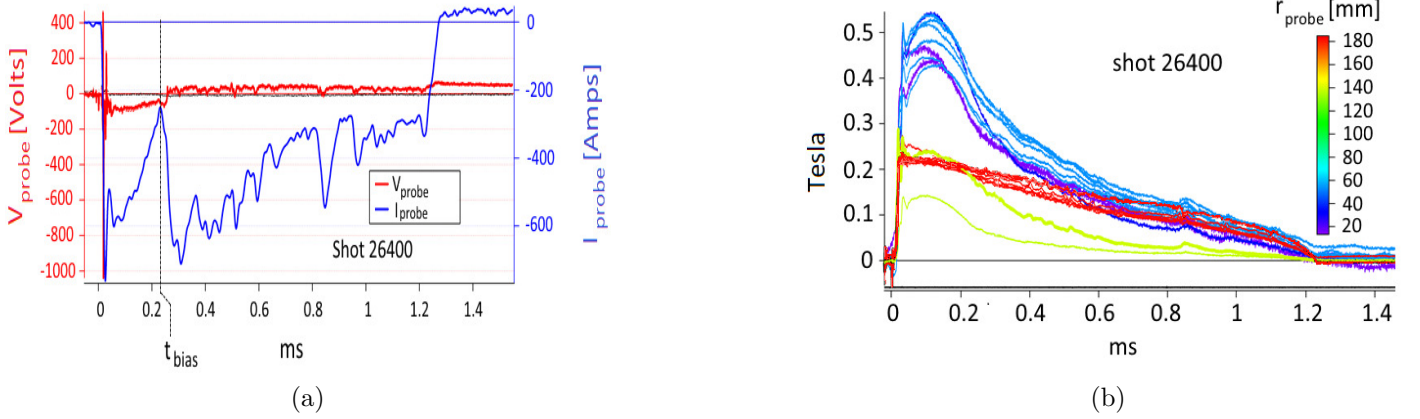


Figure 4: Measured bias probe voltage and current (a), and poloidal field (b) for shot 26400, which had $V_{bc0} = 700\text{V}$ (3mF capacitor). Note that poloidal field data is colored by magnetic probe radius.

Figure 4(a) shows the voltage measured between the probe and the vacuum vessel, and the current drawn through the plasma edge, as measured with the Rogowski coil indicated in figure 3, for shot 26400. At the biasing capacitor voltage found to be most optimal for CT lifetime and electron temperature (as obtained with the TS system), the voltage measured between the probe and vacuum vessel was typically $V_{probe} \sim +50\text{V}$ to $+80\text{V}$, and the maximum radial current drawn to the probe from the wall was $I_{probe} \sim 700\text{A}$ to $\sim 1\text{kA}$ shortly after firing the biasing capacitor(s). For shot 26400, the electrode was inserted 11mm into the edge plasma, and biased at $t_{bias} = 230\mu\text{s}$ after firing the formation capacitor banks, as indicated in figure 4(a). Note that current is already flowing through the plasma edge, and through resistor R_1 , before t_{bias} , as a result of the plasma-imposed potential on the electrode, which typically led to a measurement of $V_{probe} \sim -100\text{V}$ when magnetized plasma first enters the CT confinement area at around $20\mu\text{s}$. V_{probe} and I_{probe} decrease over time at a rate that depends on plasma and circuit parameters. Figure 4(b) indicates, for shot 26400, the poloidal field measured at the magnetic probes indicated as red dots in figure 1(a). It is interesting that the fluctuations in B_θ , which are thought to be associated with internal reconnection events, are also manifested on the biasing voltage and current measurements, *e.g.*, at $\sim 845\mu\text{s}$ in figures 4(a) and (b). This observation is enabled by the presence of the small parallel R_1 . As edge plasma impedance varies, as determined by internal MHD events, the system can divert varying proportions of capacitor driven current through R_1 . In future studies, it may be possible to influence the behaviour of the internal modes that cause the B_θ fluctuations, by driving an edge current that is resonant with the fluctuations.

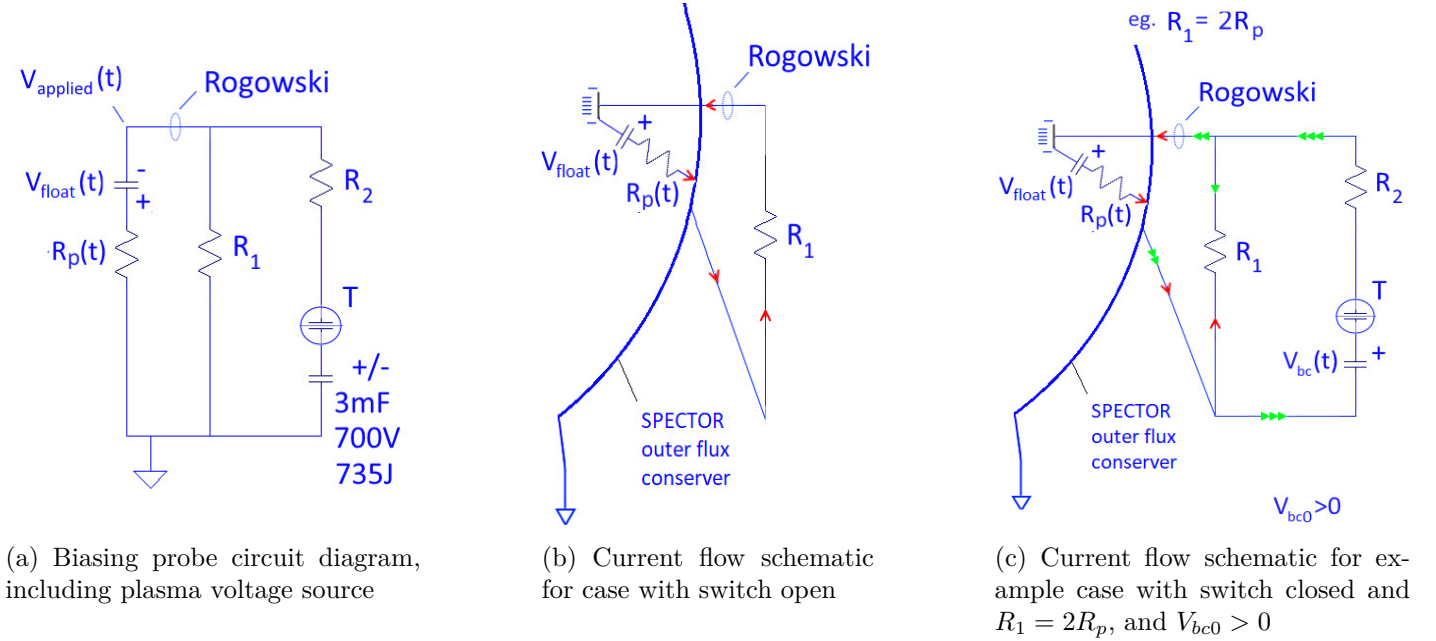


Figure 5: Biasing probe circuit diagram, including plasma voltage source, with current flow schematics

When the plasma is considered as a time-dependent voltage source, which biases the probe to floating potential $V_{float}(t)$, a more complete circuit diagram is as depicted in figure 5(a). The inclusion of R_1 , a small external resistance in parallel with R_p (the plasma resistance between the probe and wall), allows current driven by the floating potential to flow in the circuit in the case where the thyatron switch is open (see figure 5(b)). When the switch is closed, a proportion of the biasing capacitor-driven current may divert to flow through R_1 , see figure 5(c). This proportion increases as R_p increases with reducing electron temperature as the CT decays, thereby allowing I_{probe} to decrease at a rate roughly in proportion to the rate of decrease of the main CT plasma currents. The presence of an appropriately sized R_1 also prevents development of a sustained arc, which could damage the wall and probe, through the ambient plasma that remains between the probe and wall after the CT has extinguished. In previous edge biasing studies on tokamaks, the standard is to maintain approximately constant $V_{applied}$ and I_{probe} for an extended time which is a segment of the duration over which the approximately constant externally driven toroidal plasma current flows. On SPECTOR plasmas, the plasma currents are not driven and are allowed to decay naturally after formation, so a circuit configuration that establishes constant $V_{applied}$ and I_{probe} would not be compatible.

The differential voltage measured between the probe and flux conserver is

$$V_{probe}(t) = V_{applied}(t) + V_{float}(t) \quad (4)$$

If the bias capacitor is not fired, and R_1 is removed from the circuit, then in the open circuit condition $V_{probe}(t) = V_{float}(t)$. Note that V_{float} is not measured directly on each shot, however, looking at the V_{probe} measurements taken during several open circuit, probe-in shots, the floating potential can be approximated as an RC rise of the form

$$V_{float}(t) = V_{f0} e^{-\frac{t}{\tau_{RCf}}} \quad (5)$$

with $V_{f0} \sim -80\text{V}$, and, (depending on CT lifetime) $\tau_{RCf} \sim 1\text{ms}$. $V_{float}(t)$ rises from $\sim -80\text{V}$ at the time when plasma enters the CT confinement region, to 0V when the CT has decayed away. With this, an approximation for $V_{applied}$ can be made using equation 4. $V_{bc}(t)$, the voltage across the biasing capacitor,

was not measured directly in the experiment, but can be estimated as

$$V_{bc}(t) = V_{bc0} e^{-\frac{t}{\tau_{RCb}}} \quad (6)$$

where, for shot 26400, $V_{bc0} = 700\text{V}$ and $\tau_{RCb} = 0.5\Omega * 3\text{mF} = 1.5\text{ms}$ (resistance $R_2 = 0.5\Omega \gg R_e$). With these approximations for $V_{applied}(t)$ and $V_{bc}(t)$, an estimate of $R_p(t)$, the plasma resistance between the probe and flux conserver, is evaluated using equation 3, between $t_{bias} = 250\mu\text{s}$ until the time when the CT has decayed.

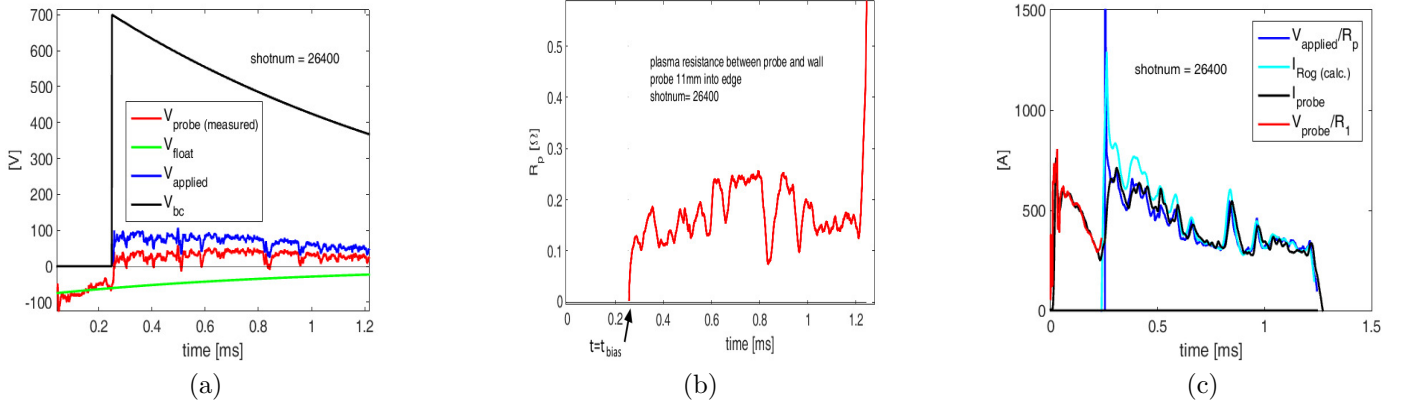


Figure 6: Calculated / measured probe voltages, edge plasma resistance and bias currents for shot 26400

The approximations (from equations 4, 5, and 6) for $V_{applied}(t)$, $V_{float}(t)$, and $V_{bc}(t)$, and measured $V_{probe}(t)$, for shot 26400, are shown in figure 6(a). Figure 6(b) shows the estimation, from equation 3, for $R_p(t)$. $R_p(t) \sim 0.15\Omega$ to 0.2Ω , and rises as T_e decreases (η_{plasma} increases) over CT decay, then drops as the edge current path length L (recall $R(t) = \eta(t)L(t)/A(t)$) decreases. Note that the current path will have a principal component along the helical magnetic field between the probe (with insertion depth 11mm) and the flux conserver. Path length decreases because B_θ decreases faster than B_ϕ (CT toroidal field is maintained at a relatively constant level by the crow-barred external shaft current) as the CT decays, *i.e.*, q increases - there are fewer poloidal transits for each toroidal transit along the path which defines R_p . The sharp dip in R_p at $t \sim 845\mu\text{s}$ coincides with the fluctuations in $I_{probe}(t)$ and B_θ seen in figures 4(a) and (b). Note that the current through the path enclosed by the Rogowski coil depicted in figures 3 and 5 can be calculated using basic circuit theory as:

$$I_{rog (calc.)} = \frac{1}{R_p(t)} \left[\frac{R_2 (V_{bc}(t) R_1 + V_{float}(t) R_1 + V_{bc}(t) R_p(t))}{R_1 R_2 + R_2 R_p(t) + R_p(t) R_1} - V_{bc}(t) - V_{float}(t) \right] \quad (7)$$

Figure 6(c) compares measured $I_{probe}(t)$ (black trace) with calculated parameters, to verify the calculation of $R_p(t)$. Referring to figure 5(c), it is seen that $V_{applied}(t)/R_p(t)$ should, as is confirmed in figure 6(c) (dark blue trace), give the measured $I_{probe}(t)$ current when the switch is closed after $t = t_{bias}$. Referring to figure 5(b), $V_{probe}(t)/R_1 \sim I_{probe}(t)$ when the switch is open before $t = t_{bias}$ (red trace in 6(c)). A good match to measured $I_{probe}(t)$ is found by using calculated $R_p(t)$ and the estimated profile of $V_{float}(t)$ in equation 7 (after $t = t_{bias}$, cyan trace). A good estimate of $R_p(t)$ is useful for optimizing external circuit resistances.

4 Main results

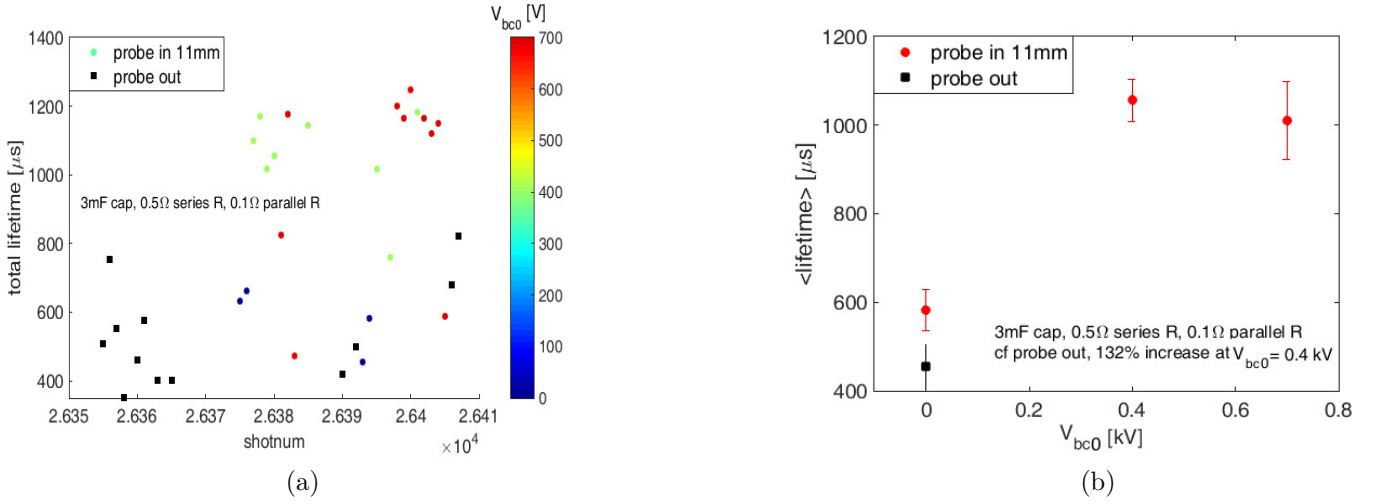


Figure 7: 3mF capacitor: total CT lifetimes *cf.* V_{bc0} (bias capacitor voltage setting)

Figure 7(a) indicates how CT lifetimes varied with V_{bc0} (coloured circles) for shots taken with the biasing probe inserted 11mm into the plasma edge in the configuration using the 3mF biasing capacitor circuit, with $R_1 = 0.1\Omega$ and $R_2 = 0.5\Omega$, compared with shots taken with the probe removed (black squares). Figure 7(b) indicates the average of CT lifetimes for the probe-out configuration (black squares), and the averages for the probe-in configuration (red circles) for the setpoints $V_{bc0} = 0\text{V}$, 400V, and 700V, where the error bars are defined with the standard error. It is indicated that CT lifetime increased from around 450 to 600eV even when the biasing capacitor was not fired - in that case, the presence of the resistor (R_1) in parallel with the biasing capacitor enables current, driven by the potential applied by the plasma, to flow from the electrode to the wall. At $V_{bc0} = 400\text{V}$, CT lifetime increased by a factor of around 2.3, from $\sim 460\mu\text{s}$ to $\sim 1070\mu\text{s}$. Note that TS data is not available for the configuration with the 3mF capacitor in the biasing circuit.

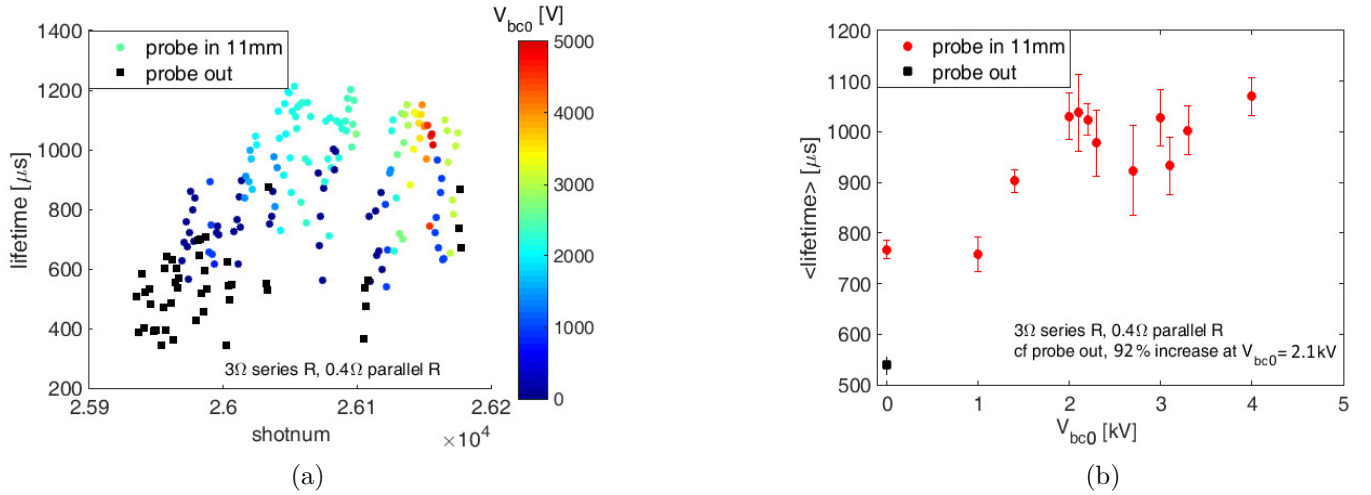
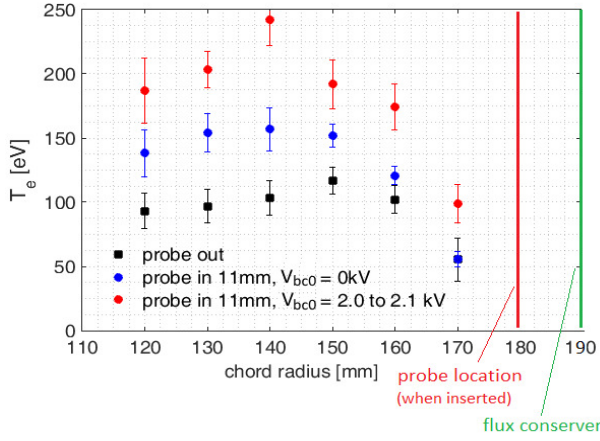
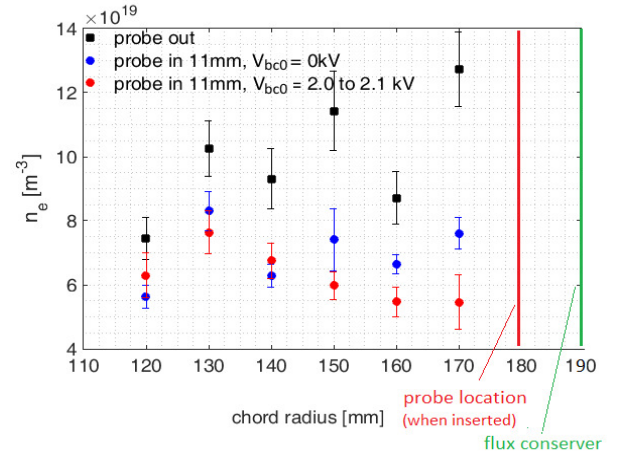


Figure 8: 100 μF capacitor: CT lifetimes *cf.* V_{bc0}

Figure 8 shows equivalent information for shots taken with a 100 μF , 5kV capacitor in the biasing circuit, with $R_1 = 0.4\Omega$ and $R_2 = 3\Omega$ (TS data is available for this configuration). CT lifetimes were approximately doubled in this configuration, with an optimal biasing capacitor setpoint of $V_{bc0} \sim 2\text{kV}$.



(a)



(b)

Figure 9: 100 μ F capacitor: electron temperature and density profiles from the Thomson scattering diagnostic at 300 μ s, for $V_{bc0} \sim 2$ kV. Note that the Thomson scattering sampling points are depicted in figure 12(b).

Figure 9 shows shot data indicating the temperature and density profiles obtained with the TS system at 300 μ s after firing the formation capacitor banks, for the configuration with the 100 μ F, 5kV biasing capacitor. Note that the TS sampling points are indicated in figure 12(b). With $V_{bc0} \sim 2$ kV, the measurements indicate that temperature is more than doubled at the inner sampling points, increasing by a factor of around 2.4 at the sampling point at $r = 140$ mm, (black squares *cf.* red circles) and the proportional increase in temperature falls off towards the CT edge. Note that current drawn through the CT edge leads to a temperature increase even when no voltage is externally applied to the electrode (black squares *cf.* blue circles). Referring to figure 9(b), electron density is markedly reduced when the electrode is inserted and the reduction is enhanced when the electrode is externally biased. It can be seen how the density profile is quite hollow without biasing, with the density highest towards the plasma edge. With biasing, a centrally peaked density profile is observed. Without biasing, the electron temperature profile is peaked at around 150mm (figure 9(a)). The electron temperature profile become more peaked, and the peak moves inwards to around 140mm when biasing is applied. It may be inferred that the pressure profile also becomes more centrally-peaked with biasing. The proportional decrease in density is greater towards the CT edge, consistent with the theory that edge fueling impediment due to an edge transport barrier is largely responsible for the density reduction (see appendix A). The diagnostic indicates an electron density reduction by factors of approximately 1.5 and 2.3 at $r = 130$ mm and $r = 170$ mm respectively.

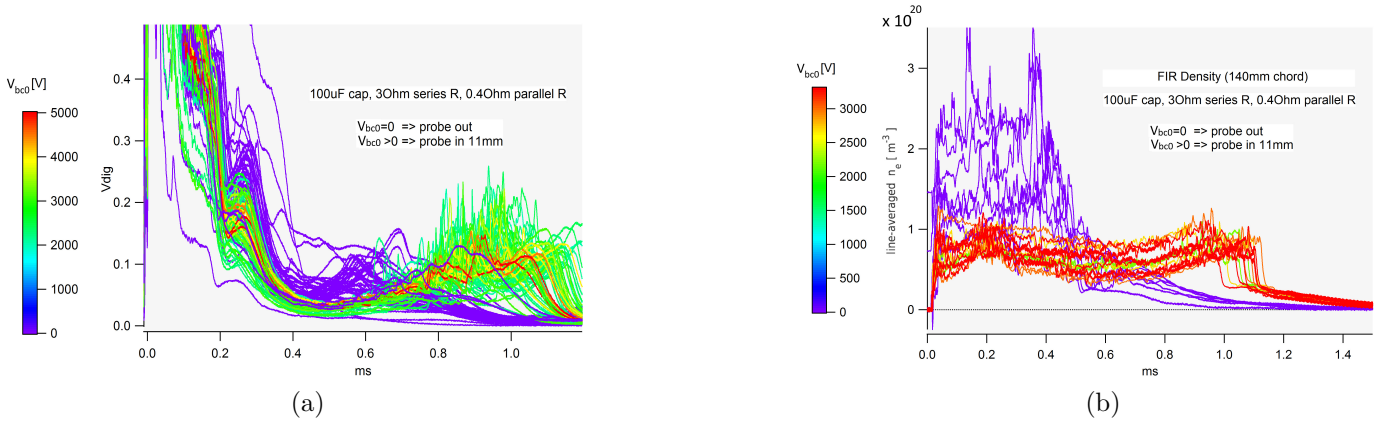


Figure 10: 100μF capacitor: (a) H_α intensity, (b) electron density (FIR interferometer)

Figure 10(a) indicates how H_α intensity, along a vertical chord located at $r = 88\text{mm}$, is reduced when the electrode is inserted and biased. Ions and electrons, that diffuse out of the plasma to the vessel walls, cool and recombine at the walls to form neutral atoms, which can then exhibit H_α emission, before being re-ionized and recycled back into the plasma as cold ions and electrons. The presence of a transport barrier reduces the level of H_α emission by reducing the flux of charged particles to the vessel walls. H_α intensity reduction is a sign of reduced recombination at the vessel walls [2]. It is thought that the reduction of the level of recombination observed may be associated with a establishment of a transport barrier due to shearing effects, and consequent reduction of flux of plasma particles from the CT core towards the vessel walls. The purple traces are from shots with the electrode removed from the vacuum vessel. As shown in figure 10(b), time-resolved FIR interferometer data from the chord at 140mm (FIR chord locations are indicated in figure 12(a)) confirms the reduction in electron density when the biased probe is inserted into the plasma edge. Again, the purple traces are from shots taken with the electrode retracted. This density reduction is thought to be due to the effect of the transport barrier impeding the level of CT fueling associated with neutral gas diffusing up the gun, as discussed in appendix A. Note that the fueling effect is not entirely eliminated by the biasing effect - density starts to increase at around 500 to 600μs (*cf.* figure 13(b)). Note that H_α intensity increases dramatically at around the same time (figure 10(a)). The CTs associated with the purple traces (probe-out configuration) in figure 10(a) and (b) do not last for long enough to enable observation of the density and H_α intensity increases at that time.

5 Discussion and conclusions

Significant increases in CT lifetime and electron temperature, and reductions in electron density and H_α intensity, were observed when the electrode was inserted into the plasma edge, even when the biasing capacitor was not fired. In that case, the presence of the resistor (R_1) in parallel with the biasing capacitor enables current, driven by the potential applied by the plasma, to flow from the electrode to the wall. Note that in cases where the biasing capacitor was not fired, the enhanced performance was eliminated when R_1 was removed from the circuit. In terms of enhanced CT lifetime, which was observed to increase by a factor of up to 2.3, the optimal biasing circuit tested was with the 3mF capacitor in place, but TS data was not available in that configuration. Up to $\sim 1200\text{A}$ was drawn 11mm through the edge plasma, while improving CT lifetime and temperature. CT lifetimes and electron temperatures were observed to increase by factors of around 2 and 2.4 (temperature near the CT core) respectively in the configuration with the 100μF capacitor charged to 2.1kV, while density decreased by a factor of around 2.3 near the CT edge. This density reduction and peaking of the originally hollow density profile

is thought to be due to the effect of a transport barrier, induced by the effect of the velocity shear caused by the imposed radial electric field, impeding the level of CT fueling associated with neutral gas diffusing up the gun (see appendix A). The consequent reduction of cool particle flux towards the CT interior is thought to be largely responsible for the particularly significant increases in observed temperature. In contrast, prior edge biasing experiments in tokamaks generally show an increase in density with no significant change in temperature. In those cases, the transport barrier results in improved energy and particle confinement, but the increase in energy is offset by the increase in particle count, so that convincing temperature increases are not observed.

The total power associated with the biasing can be estimated as $P_{bias} = V_{probe} I_{probe}$. For shot 26400 (figure 4(a)), this can be estimated as $P_{bias} \sim 35\text{kW}$ (at $300\mu\text{s}$, when $V_{probe} \sim 50\text{V}$ and $I_{probe} \sim 700\text{A}$). Typical loop voltages associated with the SPECTOR injector are of the order of 3 Volts, while plasma current was around 300kA for shot 26400 at $300\mu\text{s}$, so that the Ohmic heating power is approximately $P_{\Omega} \sim 1\text{MW}$. It appears that any plasma heating associated with the power injected by biasing would not be significant compared with the Ohmic heating power, and cannot be responsible for the observed increases in electron temperature.

Note that the biasing experiment was conducted without a fresh lithium coating on the inside of the SPECTOR flux conserver. With a fresh coating, CT lifetimes are typically around 2ms. The biasing experiment may be run again with a fresh coating. The experiment was conducted over a short period (less than two weeks). As the majority of the probe-out shots were taken at the beginning of each day, there is likely some data skew due to cleaning effects. The improvement shown with biasing may be extended with further circuit optimization. Negative biasing was tested briefly - a slight increase of electron temperature and a peaking of the electron temperature profile was observed, but there was no evidence of lifetime increase. It may be that the ion-sputtering of the probe associated with negative biasing lead to performance degradation associated with plasma impurities that offset the improvement associated with the establishment of a transport barrier. Perhaps more cleaning shots are required to see a significant improvement with negative biasing - the efficacy of negative biasing hasn't been confirmed. An IV curve was produced with the electrode biased to a range of positive and negative voltages on a shot to shot basis. Langmuir analysis indicated $T_e \sim 130\text{eV}$ and $n_e \sim 10^{19}[\text{m}^{-3}]$ at the probe location at $300\mu\text{s}$, and $T_e \sim 85\text{eV}$ and $n_e \sim 5 \times 10^{18}[\text{m}^{-3}]$ at $600\mu\text{s}$. Compared with TS data, the electron temperature estimates in particular appear too high. The fact that probe biasing affects electron temperature and electron density makes the Langmuir analysis results dubious at best, but it may be possible to correct for this effect.

It would be worth repeating the experiment with a fresh lithium coating on the inner flux conserver. Circuit parameters, probe insertion depth, and machine operation settings should be optimized further. Future SPECTOR biasing experiments would ideally have more diagnostics available so that the effects of biasing on edge conditions (for example, profiles of electric field, density, temperature edge, and plasma velocity) can be characterised using Langmuir and Mach probes, and ion Doppler diagnostics. Negative biasing may be tested more rigorously. It would be interesting to look at the effects of driving edge current resonant to the MHD behaviour that manifests itself in the form of fluctuations on measurements including CT poloidal field.

The biasing experiment was especially noteworthy because it has generally been found that insertion of foreign objects, such as thin alumina tubes containing magnetic probes, into SPECTOR CTs, leads to performance degradation associated with plasma impurities. After the extensive problems encountered relating to plasma/material interaction and impurities during the magnetic compression experiment [23, 24], special care was taken to choose a plasma-compatible material for the biasing electrode assembly. The pyrolytic boron nitride tube and molybdenum electrode combination seems to have been a good choice - at least the benefit due to drawing a current through the CT edge outweighed any performance degradation that may have been associated with impurities introduced to the system.

6 Acknowledgments

Funding was provided in part by General Fusion Inc., Mitacs, University of Saskatchewan, and NSERC. Particular thanks to Alex Mossman, Kelly Epp, Akbar Rohollahi, Russ Ivanov, and Adrian Wong for machine operation support, to Russ Ivanov, Ivan Khalzov, and Meritt Reynolds for useful discussions, and to Wade Zawalski, Curtis Gutjahr, Blake Rablah, James Wilkie, Alan Read, Mark Bunce, Pat Carle and Bill Young for hardware and diagnostics support.

A Appendix: Simulation of interaction between neutral and plasma fluids in SPECTOR geometry

It is usual to observe a significant rise in electron density at around 500 μ s on the SPECTOR machine, and it is thought that this may be a result of neutral gas, that remains around the gas valve locations after CT formation, diffusing up the gun. Ionization of the neutral particles would lead to CT fueling and an increase in observed electron density. An energy, particle, and toroidal flux conserving finite element axisymmetric MHD code was developed to study CT formation into a levitation field, and magnetic compression [23, 24, 25]. The Braginskii MHD equations with anisotropic heat conduction were implemented. As described in [23, 26], a plasma-neutral interaction model including ionization, recombination, charge-exchange reactions, and a neutral particle source, was implemented to the MHD code and used to study the effect of neutral gas on simulated CT formation in SPECTOR geometry.

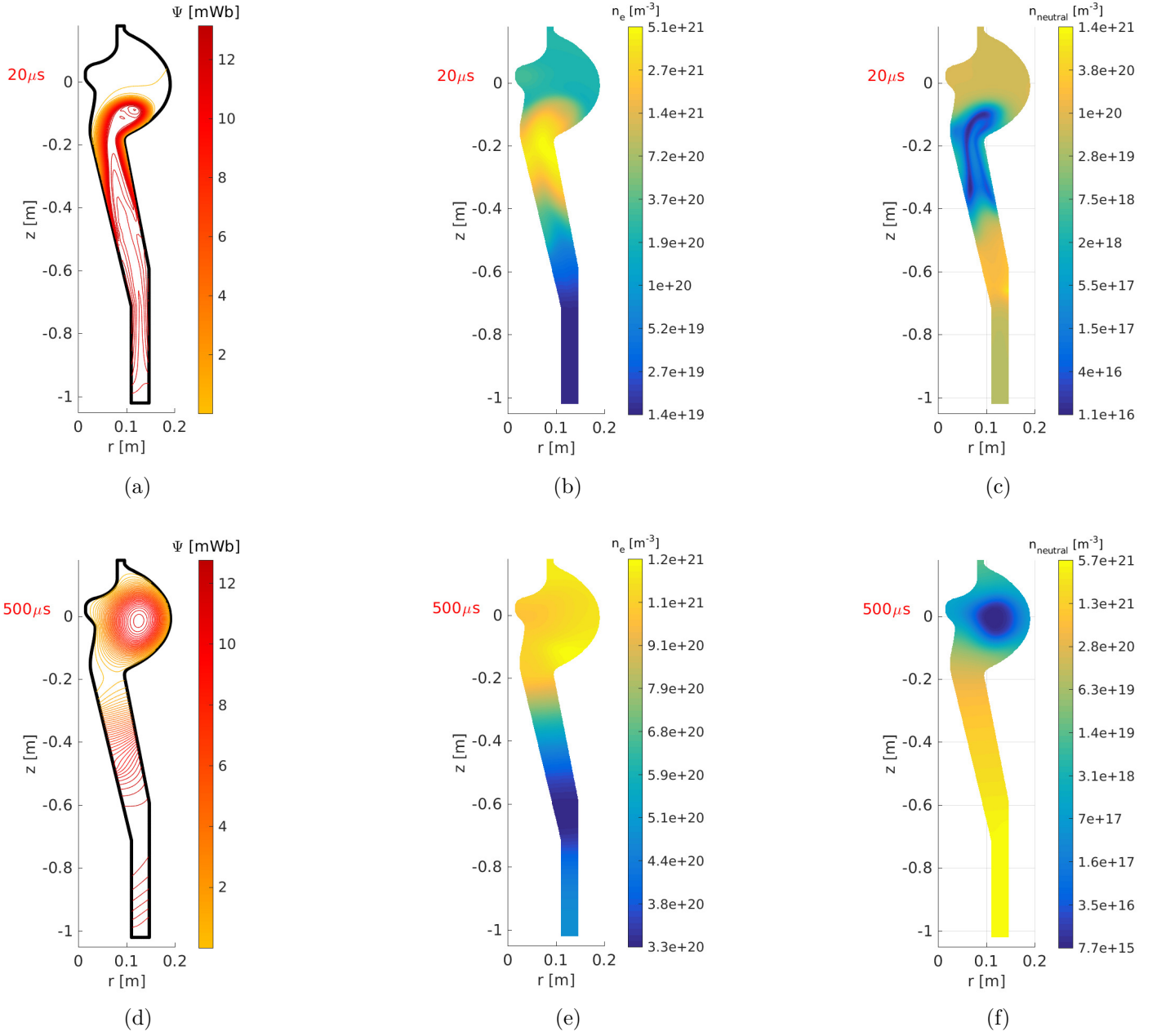


Figure 11: Poloidal flux contours and profiles of electron and neutral fluid densities at various times from a simulation of CT formation in the SPECTOR plasma injector

Figures 11(a), (b) and (c) show ψ contours and profiles of n_e and n_n at $20\mu\text{s}$, as plasma enters the CT containment region. Profiles of the same quantities are shown in figures 11(d), (e) and (f) at $500\mu\text{s}$, around the time when the rise in measured electron density is usually observed. It can be seen how neutral fluid density is highest at the bottom of the gun barrel - any neutral gas advected or diffusing upwards is ionized. A region of particularly high electron density is apparent just above, and outboard of, the entrance to the containment region - this is due to the fueling effect arising from neutral gas diffusion.

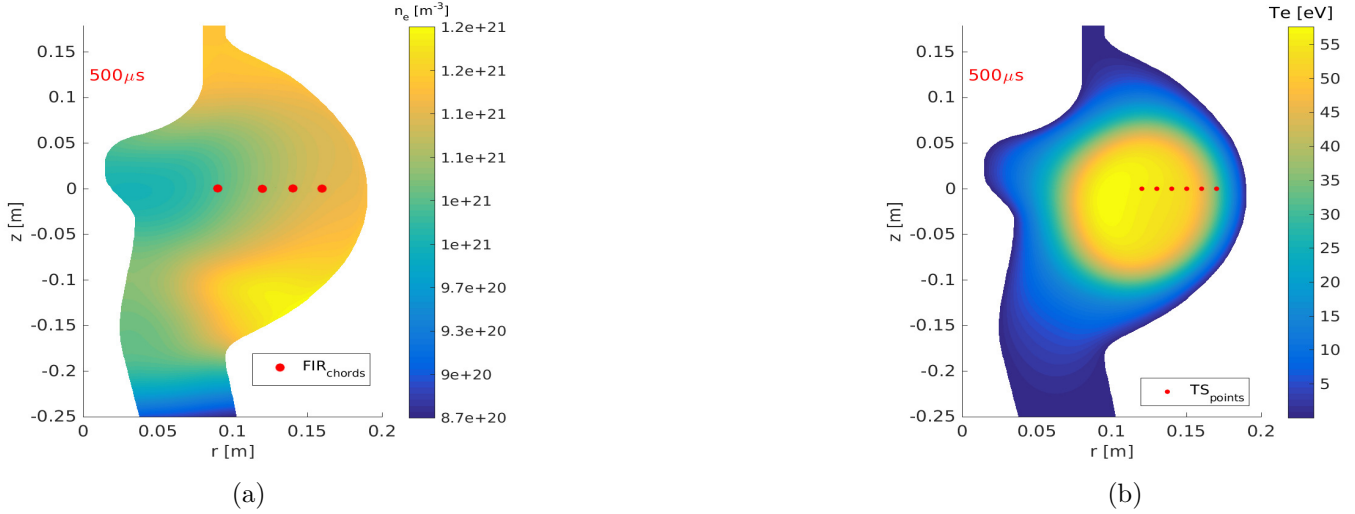


Figure 12: Profiles of electron density and temperature at $500\mu\text{s}$ from a simulation of CT formation in the SPECTOR plasma injector

The region of particularly high electron density is more defined in figure 12(a), in which cross-sections of the horizontal chords representing the lines of sight of the FIR (far-infrared) interferometer [22] are also depicted. The electron temperature profile at $500\mu\text{s}$ is shown in figure 12(b). Referring to figure 11(f), it can be seen how neutral fluid density is low in regions of high T_e as a result of ionization.

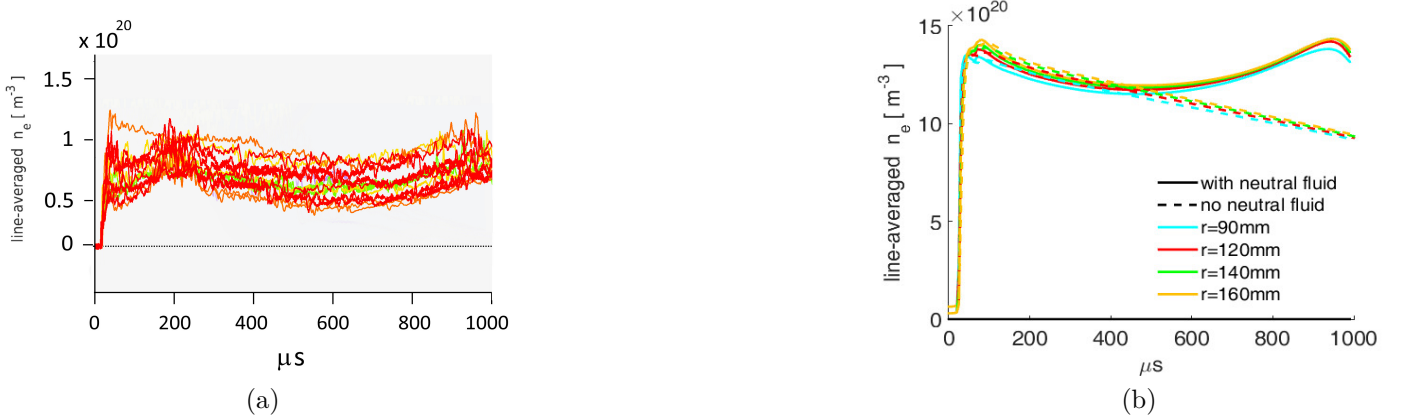


Figure 13: Effect of neutral fluid dynamics in SPECTOR geometry

Figure 13(a) shows measured line-averaged electron density along the chord at $r = 140\text{mm}$ from a selection of several shots in SPECTOR. It can be seen how density starts to rise at around 500 to $600\mu\text{s}$. Figure 13(b) shows the simulated diagnostic for line-averaged electron density along the chords indicated in figure 12(a). The density rise is qualitatively reproduced when a neutral fluid is included in the simulation. Similar simulations without the inclusion of neutral fluid do not indicate this density rise (dashed lines in figure 13(b)). Note that the simulations presented in figure 13(b) were run with artificially high plasma density in order to allow for an increased timestep and moderately short simulation run-times. Hence, the electron temperatures indicated in figure 12(b) are underestimations of the actual temperatures due to the overestimation of density in the simulation. The main goal of these simulations was to demonstrate that the inclusion of neutral fluid interaction can qualitatively model the observed electron density increase.

References

- [1] F. Wagner, G. Becker, K. Behringer, D. Campbell, A. Eberhagen, W. Engelhardt, G. Fußmann, O. Gehre, J. Gernhardt, G. von Gierke et al., *Regime of Improved Confinement and High Beta in Neutral-Beam-Heated Divertor Discharges of the ASDEX Tokamak*, Phys. Rev. Lett. 49 1408 (1982)
- [2] R. J. Taylor, M. L. Brown, B. D. Fried, H. Grote, J. R. Liberati, G. J. Morales, and P. Pribyl, *H-Mode Behavior Induced by Cross-Field Currents in a Tokamak*, Phys. Rev. Lett. 63 2365 (1989)
- [3] R. Weynants and R. Taylor, *Dynamics of H-mode-like edge transitions brought about by external polarization*, Nucl. Fusion 30 945 (1990)
- [4] R. J. Groebner, K. H. Burrell, P. Gohil, and R. P. Seraydarian, *Spectroscopic study of edge poloidal rotation and radial electric fields in the DIII-D tokamak (invited)*, Review of Scientific Instruments 61, 2920 (1990)
- [5] F. Zacek, J. Stockel, L. Kryska, K. Jakubka, J. Badalec, and I. Duran, *Preliminary experiments with edge plasma biasing in tokamak CASTOR*, Czech. J. Phys. 48 60 (1998)
- [6] G. Van Oost, J. P. Gunn, A. Melnikov, J. Stockel, and M. Tendler, *The role of radial electric fields in the tokamaks TEXTOR-94, CASTOR, and T-10*, Czechoslovak Journal of Physics 51: 957 (2001)
- [7] G.S. Kirnev, S.A. Grashin, L.N. Khimchenko, and N.N. Timchenko, *First results of biasing experiments on the T-10 tokamak*, Czechoslovak Journal of Physics 51: 1011 (2001)
- [8] W. Zhang, C. Xiao, and A. Hirose, *Plasma autobiasing during Ohmic H-mode in the STOR-M tokamak*, Physics of Fluids B: Plasma Physics 5, 3961 (1993)
- [9] H. Figueiredo, I. S. Nedzelskiy, C. Silva, C. A. F. Varandas, J. A. C. Cabral, and R. M. O. Galvão, *Electron emissive electrode for the plasma biasing experiment on tokamak ISTTOK*, Review of Scientific Instruments 75, 4240 (2004)
- [10] S. Jachmich, G. Van Oost, R. R. Weynants, and J. A. Boedo, *Experimental investigations on the role of ExB flow shear in improved confinement*, Plasma Phys. Control. Fusion 40 1105, (1998)

- [11] Y. Sun, Z. P. Chen, T. Z. Zhu, Q. Yu, G. Zhuang, J. Y. Nan, X. Ke, H. Liu, and the J-TEXT Team, *The influence of electrode biasing on plasma confinement in the J-TEXT tokamak*, Plasma Phys. Control. Fusion 56 015001 (2014)
- [12] I.C. Nascimento, Y.K. Kuznetsov, J.H.F. Severo, A.M.M. Fonseca, A. Elfimov, V. Bellintani, M. Machida, M.V.A.P. Heller, R.M.O. Galvão, E.K. Sanada et al., *Plasma confinement using biased electrode in the TCABR tokamak*, Nucl. Fusion 45 796 (2005)
- [13] M. Tendler, *Different scenarios of transitions into improved confinement modes*, Plasma Physics and Controlled Fusion, vol. 39, no. 12, pp. B371–B382 (1997)
- [14] K. Burrell, *Tests of causality: Experimental evidence that sheared flow alters turbulence and transport in tokamaks*, Phys. of Plasmas 6, 4418 (1999)
- [15] E. Waltz, G. D. Kerbel, J. Milovich, and G. W. Hammett, *Advances in the simulation of toroidal gyro-Landau fluid model turbulence*, Phys. Plasmas 2, 2408 (1995)
- [16] S. Cowley and R. Kulsrud, *Considerations of ion-temperature-gradient-driven turbulence*, Phys. Fluids B, 3 (10) (1991)
- [17] K C Shaing, C T Hsu, and P J Christenson, *Model for the L-H transition in Tokamaks*, Plasma Physics and Controlled Nuclear Fusion Research, Proceedings of the 12th International Conference, Nice, France
- [18] H. Biglari, P. Diamond, and P. Terry, *Influence of sheared poloidal rotation on edge turbulence*, Physics of Fluids B: Plasma Physics 2, 1 (1990)
- [19] N. P. Basse, S. Zoletnik, G. Y. Antar, J. Baldzuhn, A. Werner, and the W7-AS Team, *Characterization of turbulence in L- and ELM-free H-mode Wendelstein 7-AS plasmas*, Plasma Phys. Control. Fusion 45 439 (2003)
- [20] S. Howard, *Experimental results from the SPECTOR device at General Fusion*, oral presentation at 27th IEEE Symposium on Fusion Engineering (2017) (available at <https://generalfusion.com/2017/06/experimental-results-spector-device-general-fusion-sofe-2017/>)
- [21] W. C. Young and D. Parfeniuk, *Thomson scattering at general fusion*, Rev. Sci. Instrum. 87, 11E521 (2016)

- [22] P. Carle, A. Froese, A. Wong, S. Howard, P. O'Shea, and M. Laberge, *Polarimeter for the General Fusion SPECTOR machine*, Rev. Sci. Instrum. 87, 11E104 (2016)
- [23] C. Dunlea, *Magnetic Compression of Compact Tori - Experiment and Simulation*, Ph.D. dissertation (University of Saskatchewan, 2019)
- [24] C. Dunlea, S. Howard, W. Zawalski, K. Epp, A. Mossman, General Fusion Team, Chijin Xiao, Akira Hirose, *Magnetic Levitation and Compression of Compact Tori*, available at arXiv:1907.10307, submitted to Physics of Plasmas (2019)
- [25] C. Dunlea and I. Khalzov, *A globally conservative finite element MHD code and its application to the study of compact torus formation, levitation and magnetic compression*, available at arXiv:1907.13283, submitted to J. Comp. Phys. (2019)
- [26] C. Dunlea, C. Xiao, and A. Hirose, *A model for plasma-neutral fluid interaction and its application to a study of CT formation in a magnetised Marshall gun*, submitted to Physics of Plasmas (2019)